Pulsed Nd:YAG Laser Surface Texturing of Pure Titanium Material

G. Kibria, A. Sen, H. M. Tariq Aziz, B. Doloi and B. Bhattacharyya

Abstract Laser surface texturing is one of the key technologies in micromachining domain for generating defined surface features in micro-components in recent times. In this process, highly focused laser beam is irradiated on the material surface and laser scanning is carried out at different scanning patterns to alter surface conditions for improving the tribological properties of that surface. In this research study, an attempt has been made to carry out laser surface texturing on pure titanium material having a thickness of 1 mm with the aid of a pulsed Nd:YAG laser system. The various process parameters considered for the present research works are laser beam average power, pulse frequency, laser beam scanning speed, and transverse feed. Utilizing response surface methodology, experimentation has been planned. The responses measured are surface roughness, Ra and Rz in lateral and transverse directions and contact angle (θ). The chapter also highlights experimental results for validation of the developed empirical models. The test results have been analyzed using various surface plots. Multi-performance optimization has been conducted to obtain minimum values of surface roughness and contact angle. Using optical microscopic images, influence of process parameters on responses have also been discussed.

Keywords Laser surface texturing · Pulse Nd:YAG laser · Titanium Surface roughness · RSM · Optimization · Contact angle

G. Kibria (✉) · H. M. Tariq Aziz
Mechanical Engineering Department, Aliah University, Kolkata 700156, India
e-mail: prince_me16@rediffmail.com

H. M. Tariq Aziz
e-mail: hazaritariq@gmail.com

A. Sen · B. Doloi · B. Bhattacharyya
Production Engineering Department, Jadavpur University, Kolkata 700032, India
e-mail: abhishek.sen1986@gmail.com

B. Doloi
e-mail: bdoloionline@rediffmail.com

B. Bhattacharyya
e-mail: bb13@rediffmail.com

S. S. Pande and U. S. Dixit (eds.), *Precision Product-Process Design and Optimization*, Lecture Notes on Multidisciplinary Industrial Engineering,
https://doi.org/10.1007/978-981-10-8767-7_14

1 Introduction

The present era belongs to the utmost demand of minimization of the products with the requirement of stringent quality control. The margin of era for fabricating miniaturized products almost tends to zero. The demand of micro-products in the area of automotive, biomedical, and aerospace engineering is ever increasing. Therefore, a number of micromachining processes have been developed successfully in order to meet those demands (Gentili 2005). Furthermore, several micromachining strategies have also been implemented successfully to manufacture micro-parts with high accuracy, reliability, and durability. With the progress of material science research, various high strength and temperature resisting (HSTR) materials are being developed for successfully implementing them in product manufacturing (Jackson 2015; Ali 2017). Laser beam micromachining processes are being utilized for micromachining of superalloys to advanced newly developed materials to meet the utmost demand from the industries like micro-reactors, electronics, biomedical, chemical and sensors–actuators (Meijer 2004; Chang et al. 2012). The laser micromachining approaches toward generating precise micro-features on the difficult to machine materials have a great potential to generate complicated featured micro-products with several unique characteristics such as high potentiality and effectiveness, exclusion of finishing stages, better quality products, higher material utilization and coverage, material processing regardless of its electrical conductivity, etc. (Mishra and Yadava 2015; Chavoshi and Luo 2015). In laser micromachining processes, highly intensive laser beam is transmitted on desired location of surface of material to simultaneously melt and vaporize the material. By utilizing assisted air or gas pressure, the melted and/or vaporized materials are removed from the focused zone creating crater on the surface (Kibria 2015).

Surface texturing using high intense laser beam is a promising advanced micromachining technology for the generation of defined surface features in engineering materials to improve the tribological performance of metallic and ceramic materials (Cunha 2016; Dunn et al. 2015; Toyserkani 2014). This process is a viable technology for surface engineering that can produce significant improvement of engineering components in various aspects such as wear resistance, wetting characteristics, friction coefficients, load capacities, and part lubrication. In laser texturing process, laser beam is focused and exposed on the workpiece surface with defined patterns by relatively moving the workpiece in X and Y directions. Thus, laser beam scanning was applied on the surface with overlaps between two consecutive laser scan tracks. The amount of this overlap is controlled by the value of transverse feed. In this way, laser surface texturing is carried out on workpiece surface to obtain square or rectangular type scan area. With the change in the number of scan passes during laser surface texturing process, a specific depth as well as surface features can be achieved. In laser surface texturing process, the controllable process variables such as laser beam power, pulse frequency or pulse repetition rate, scanning speed, etc., have great effect to obtain quality and defined

surface features. These process parameters are dynamic and most of the performance criteria are expressively connected with instantaneous distinction of parameters during processing of advanced engineering materials.

Titanium is an attractive material for numerous industries such as aerospace, biomedical, sports, architecture, etc., for its diversified properties such as extremely tough, lightweight, high strength to weight ratio, corrosion resistance, biological compatibility, low density, low coefficient of thermal expansion, stability at elevated temperature, etc. Pure titanium is one of the biologically inert biomaterials as it exhibits property of high biocompatibility with tissue and blood. Due to this, this material is largely used for fabricating biomedical implants. In the literature, limited research work has been performed by various researchers and academia in the area of laser surface texturing on different engineering materials using various types of laser. Cunha (2016) carried out research on surface texturing process by means of direct laser writing using ultrashort laser beam on titanium and Ti–6Al–4V alloy. A wide range of created textures like laser-induced periodic surface structures (LIPSS), nanorange pillars and columns and composite type textures have been studied by the authors. The researchers also found that these specific generated textures have an accumulation amount of ability of governing the wettability performance for various biological fluids and other fluids on the material surface. Kovalchenko et al. (2004) carried out tribological experiments on pin-on-disk assessment device at a sliding speed of 0.15–0.75 m/s and minimal interaction pressure of 0.16–1.6 MPa. The authors found that the surface texturing process using laser prolonged the range of speed-load factors for hydrodynamic lubrication. Li et al. (2016) established the manufacture of steady super-hydrophilic and super-hydrophobic textured titanium surface using femtosecond pulsed laser. In scanning strategy by laser in two perpendicular orders enclosed by nanometer-sized ripples, are directed for the development of spikes of micrometer size. The results show that textured hydrophilic or super-hydrophilic Ti surfaces became high hydrophobicity or super-hydrophobicity after salinization. In Fig. 1, the laser-textured surface of Ti material machined at laser fluence of 1.5 J/cm^2 is shown at two different magnifications (500× an 50000×). Soveja et al. (2008) investigated the effect of working factors on laser texturing by means of two investigational design approach (Taguchi and RSM methodology) on Ti–6Al–4V alloy. The authors found that pulse frequency and pulse energy are the most significant factors. The results also reveal that MRR is directly proportional to laser pulse energy and pulse frequency. Moreover, it was seen that these values of surface roughness were inversely relational to these process parameters. Tripathi et al. (2015) studied the influence of laser surface texturing process on friction and wear behavior of graphite cast iron. In this work, authors successfully produced dimples of dimension of diameter 60 μm and depth 30 μm with a dimple pitch of 80–200 μm.

Velasquez (2013) investigated the effect of surface texturing on the surgical blade by developing micro-dimples of diameter of 110 μm and depth of 30 μm on the surface of cutting edge of blades (surgical) by a picosecond pulse Nd:YVO4 laser. A larger friction reduction is observed by production of an arrangement of dimples with combined rims on a side of blade cutting edge in comparison with

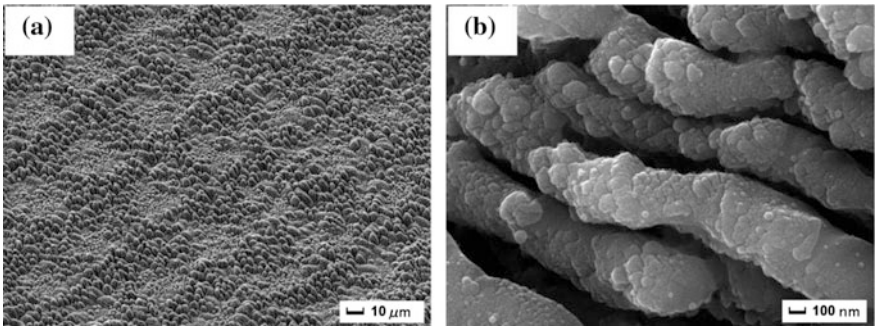

Fig. 1 SEM images of laser texturing Ti surface at **a** 500× and **b** 50000× magnifications machined at laser fluence of 1.5 J/cm^2 (Li et al. 2016)

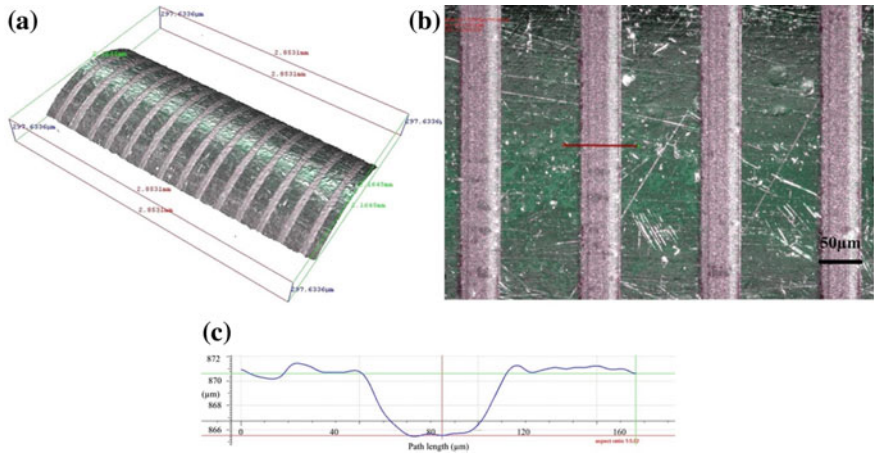

Fig. 2 3D and 2D profiles of machined micro-channels at axial overlap of 0.80, circumferential overlap of 0.88 and overscan number of 2 (Wang et al. 2015)

production of these dimples at both sides. Wang et al. (2015) carried out investigational analysis to study the effect of overlap and overscan number and found that both the factors have significant effects on results of depth achieved and surface roughness values. It was found that machined depth has a linear relationship with the axial overlap and circumferential overlap. The results also reveal that the overscan number is mostly effective factor for machined depth compared to the overlap factors. The 3D and 2D scan profiles of the micro-channel machined surface are shown in Fig. 2 at axial overlap of 0.80, circumferential overlap of 0.88 and overscan number of 2. Yang et al. (2016) studied the modification of wettability on titanium material. The results show that accumulation of carbon on the surface is the key factor to improve surface hydrophobicity. The SEM images of three type of

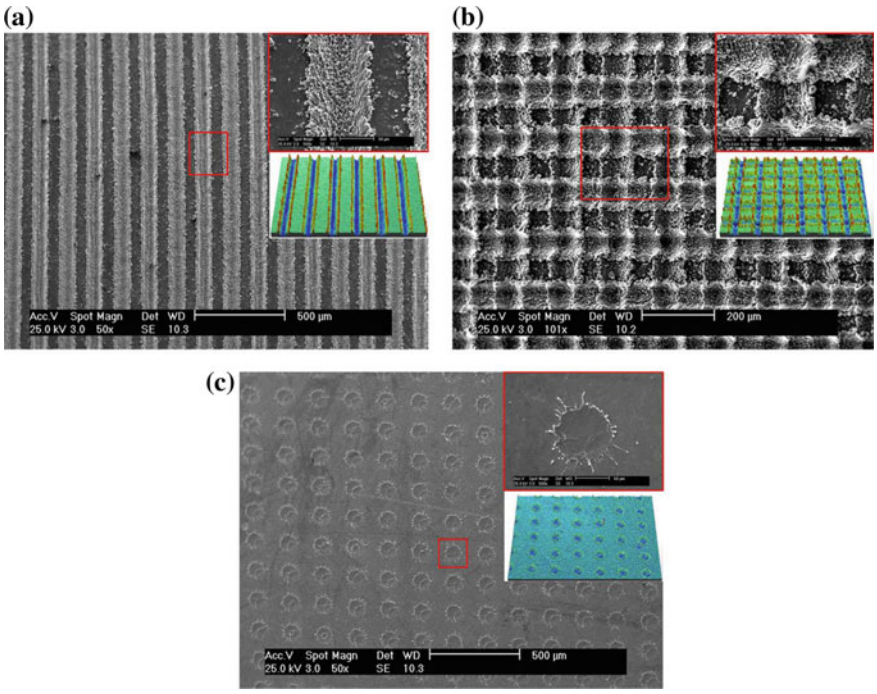

Fig. 3 SEM images of standard microstructures **a** line pattern **b** grid pattern and **c** spot pattern under the irradiation of laser pulses (Yang et al. 2016)

patterns such as line, grid, and spot patterns are shown in Fig. 3a–c. From the literature review, it was found that very few experimental researches have been carried out in order to find out the influencing process variables on surface characteristics and the effect of overlap factors on surface conditions during laser surface texturing process. Furthermore, as the process involves a number of process parameters, the selection of suitable process parameter setting is a very difficult task for achieving the desired surface characteristics. Therefore, to meet the micro-manufacturing demands and also to explore the influences of different process parameters on surface characteristics, in the present chapter, attempts have been made to conduct experiments in laser surface texturing process on titanium material to analyze the effect of laser average power, laser beam scanning speed, pulse frequency, and transverse feed on the response criteria. The research work also attempts to develop empirical models for responses through response surface methodology to analyze the effect of aforesaid process inputs. Finally, optimization has been carried out to develop optimal parametric combinations to achieve desired surface characteristics.

2 Laser Surface Texturing

One of the key technologies for manufacturing of defined and patterned surface microstructures is laser surface texturing (LST). This process renders tribological characteristics on the surface of work material to improve load capacity, wear rate as well as to reduce coefficient of friction of the surface. In this process, relative movements between the laser beam and work surface is given at different patterns to create patterned microstructures such as crossed grooves, linear grooves, and dimple-shaped impressions. In laser texturing process, lateral overlap and transverse overlap are the major criteria for achieving qualitative and defined surface. Therefore, the basic understanding of lateral overlap and transverse overlap of laser beam scanning is very much needed. The schematic representation of laser beam scan pattern with two overlaps is viewed in Fig. 4. The schematic representation also shows the Gaussian energy distributions of laser spots as well as the craters generated by these laser spots. The amount of lateral overlap and transverse overlap should be chosen very carefully as these overlaps depend upon the various parametric settings of process parameters. The mathematical relationship between various factors and the abovementioned overlaps can be calculated as follows (Vora and Dahotre 2015):

$$\text{Lateral overlap } (O_{\mathrm{L}}) = \frac{D - D_{\mathrm{L}}}{D} \times 100\% \tag{1}$$

$$\text{Transverse overlap } (O_{\mathrm{T}}) = \frac{D - D_{\mathrm{T}}}{D} \times 100\% \tag{2}$$

Here, D is the laser beam spot diameter at focused zone in mm, D_{L} ($D_{\mathrm{L}} = V_{\mathrm{in}}/f$) is lateral overlap distance in mm, V_{in} is the laser beam scanning speed in mm/s, f corresponds to pulse frequency in Hz, and D_{T} is the transverse overlap distance in mm. According to Eq. (1), it is very clear that by increasing the pulse frequency or

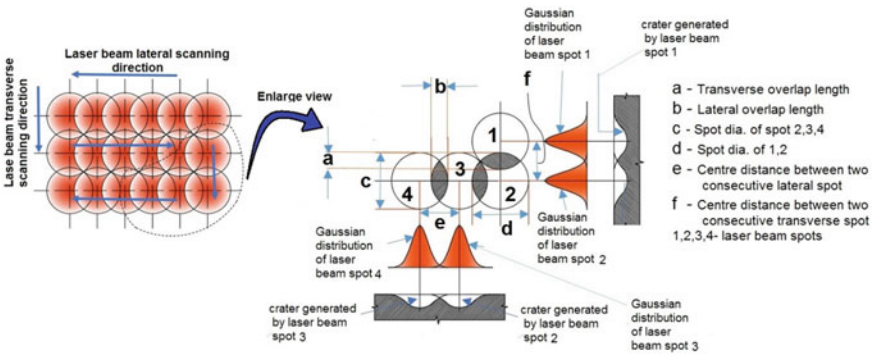

Fig. 4 Schematic view of laser scanning strategy showing lateral and transverse overlap and Gaussian energy distribution pattern for laser spots

by reducing the laser beam scanning speed, the lateral overlap area can be incremented. Equation (2) depicts the relation of transverse overlap with transverse feed. It is theoretically very clear than the transverse overlap area, i.e., overlap of two consecutive laser spot in transverse direction, can be increased by decreasing the transverse feed or reducing the center distance between two consecutive spots.

3 Materials, Methods, and Machining Conditions

All the experimentation were carried out in CNC controlled pulse Nd:YAG laser beam micromachining system of average power 50 W (make: M/S Sahajanand Laser Technology Limited, Pune, India). In the present experimental investigation, the process parameters, which have been selected for conducting laser surface texturing process of pure titanium, are average power of laser, pulse frequency, laser beam scanning speed, and transverse feed. The list of process parameters with actual and coded values is shown in Table 1. Finally, a uniform rotatable central composite experimental design based on response surface methodology (RSM) for modeling of laser surface texturing process has been carried out and listed in Table 2. The details of machine setup specifications and other parameters which are kept constant during the present experimentation are shown in Table 3. Each of the four process parameters having four levels requires a total of 31 numbers of experiments. All the experiments have been performed randomly, i.e., without following the order mentioned in the first column. Considering the ranges of process parameters taken in this research study, the values of lateral overlap and transverse overlap have been calculated using Eqs. (1) and (2). In Fig. 5, the variation of lateral overlap with laser scanning speed at various pulse frequency values is shown. From this figure, it is revealed that the values of lateral overlap are more than 95%, which ensures that quality surface can be achieved by laser surface texturing process. The variation of transverse overlap with transverse feed is shown in Fig. 6. The calculated values of transverse overlap are in the range of 50–90%. This wide range of overlap has been considered to study and analyze the effect of these overlaps on surface characteristics to be obtained. Flat titanium workpiece of

Table 1 Process parameters and various levels of laser surface texturing experimentation

Parameters	Symbol	Unit	Levels				
			−2	−1	0	+1	+2
Average power	X1	W	4	5.5	7	8.5	10
Pulse frequency	X2	Hz	600	800	1000	1200	1400
Scanning speed	X3	mm/s	1	2	3	4	5
Transverse feed	X4	mm	0.01	0.02	0.03	0.04	0.05

Table 2 Experimental plan with various values of process parameters

Expt. No.	Average power (W)	Pulse frequency (Hz)	Scanning speed (mm/s)	Transverse feed (mm)
1	7.0	1000	3	0.03
2	8.5	1200	4	0.04
3	8.5	800	2	0.04
4	5.5	800	4	0.02
5	8.5	800	4	0.04
6	5.5	1200	2	0.02
7	8.5	800	2	0.02
8	8.5	1200	2	0.02
9	7.0	1000	3	0.03
10	5.5	1200	4	0.04
11	5.5	800	2	0.04
12	7.0	1000	1	0.03
13	10.0	1000	3	0.03
14	7.0	1000	3	0.05
15	8.5	1200	2	0.04
16	7.0	1000	3	0.01
17	7.0	1000	3	0.03
18	7.0	1000	3	0.03
19	5.5	1200	2	0.04
20	5.5	1200	4	0.02
21	7.0	1000	5	0.03
22	7.0	600	3	0.03
23	7.0	1000	3	0.03
24	4.0	1000	3	0.03
25	7.0	1000	3	0.03
26	8.5	800	4	0.02
27	7.0	1000	3	0.03
28	5.5	800	4	0.04
29	7.0	1400	3	0.03
30	8.5	1200	4	0.02
31	5.5	800	2	0.02

dimension 50 mm × 50 mm × 1 mm is considered for carrying out the experimentation. After conducting experiments, response criteria surface roughness (Ra and Rz) both in lateral and transverse directions and wettability (in terms of contact angle) were measured. Surface roughness values were measured using roughness measuring instruments, Mitutoyo Surftest SJ-210. During surface roughness evaluation, the cutoff length was taken as 0.8 mm and total length of measurement was 5 mm. The values of surface roughness along the laser scan line (lateral direction) are termed as surface roughness (Ra and Rz) in lateral direction whereas the values

Table 3 Experimental conditions for laser surface texturing

Condition	Description
Laser type	Nd:YAG laser (pulsed)
Wavelength	1064 nm
Polarization of beam	Random
Type of Q-switch	Q-switched (pulsed)
Mode of operation	Fundamental mode (TEM_{00})
Mode of laser beam	Acousto optic
Pulse width, % of duty cycle	Variable
Mirror reflectivity	Rear mirror 100% and front mirror 80%
Air pressure (kgf/cm^2)	1.3
Z feed rate (mm/s)	0.01

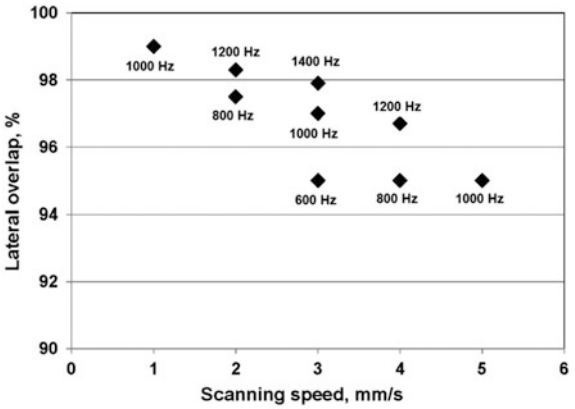

Fig. 5 Variation of lateral overlap with laser scanning speed at various pulse frequency values

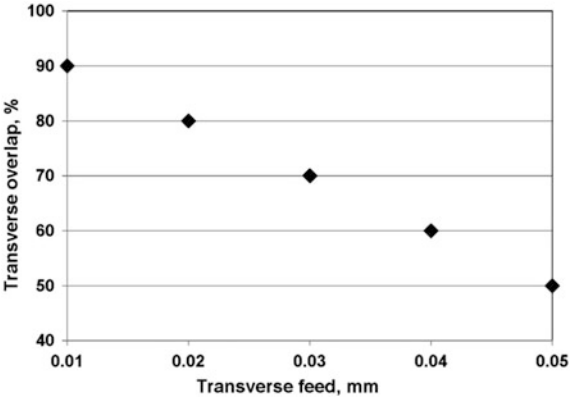

Fig. 6 Variation of transverse overlap with transverse feed

of surface roughness obtained along the perpendicular of lateral direction (i.e., transverse direction) are termed as surface roughness (Ra and Rz) in transverse direction. Wettability is another response criterion that was considered in the present experimentation. Wettability is the effect of variation of contact angle on the surface that decides whether the liquid drop over the surface is able to wet the surface or not. As this is a direct function of contact angle (θ), therefore, wettability is calculated by the angle of contact of the liquid resting on the surface. If two different fluids make contact with the surface of a solid, the configuration of balance of these two different fluid segments (say air and water) relies on the comparative value of the surface tension among every pair of these three phases. Each surface tension executes toward its respective interface, and defines the angle (θ) at which the liquid contacts the surface. This is known as contact angle. The contact angle is generally measured in the liquid side. When the contact angles are >90°, the wettability characteristics of the liquid on the surface are very low, i.e., hydrophobic. At the same time, when contact angles are <90°, the wettability characteristics are very high on the surface, i.e., hydrophilic. Even a contact angle of more than 150° shows super-hydrophobicity. Wettability of the machined surface was observed by measuring contact angle of pre-quantified distilled water drop. The schematic view of measuring the contact angle using water droplet is represented in Fig. 7. The wettability of the textured surface in terms of contact angle, angle measuring setup is indigenously developed and the schematic representation of this setup is viewed in Fig. 8. For each water drop on the machined surface, contact angle is measured twice at both ends of water drop and for analysis; the average value of these two angles is taken. MINITAB statistical software of version 16.1 is used to analyze the responses.

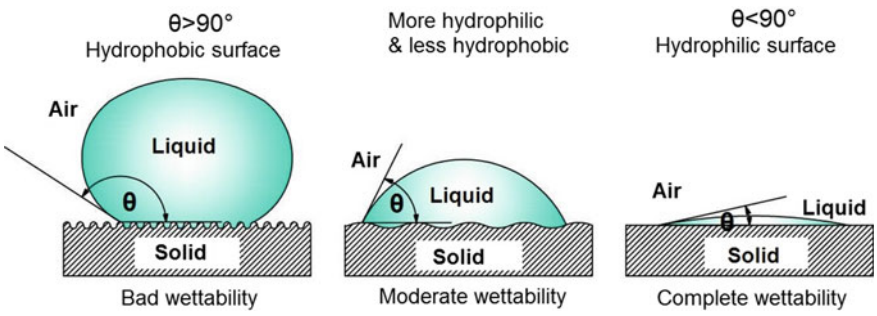

Fig. 7 Schematic of contact angle of liquid drops in contact with solid surfaces (hydrophobic and hydrophilic)

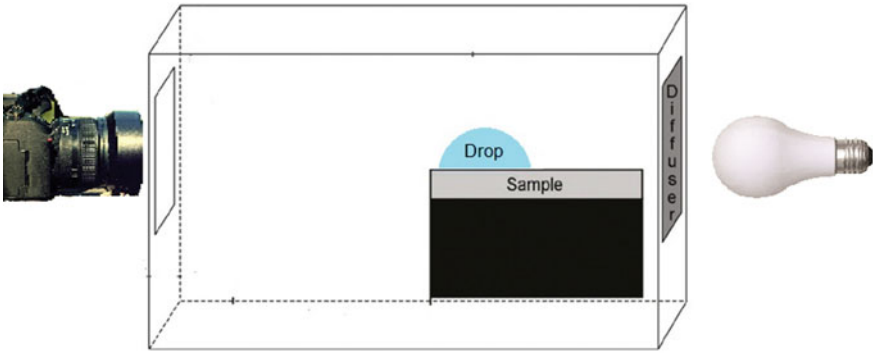

Fig. 8 Schematic view of indigenously developed contact angle measuring arrangement

4 Results and Discussion

Based on the results of laser surface texturing on pure titanium material, various statistical analyses were conducted to validate the developed mathematical models of responses. Moreover, various surface plots were analyzed to examine the parametric influences of process parameters on performance criteria.

4.1 Development of Predictive Models and ANOVA Test

According to the results of response criteria, i.e., surface roughness (Ra and Rz) and contact angle achieved as shown in Table 4, mathematical models of responses have been established to develop the relationship between various process parameters and performance criteria. The details of developed mathematical models of responses are shown below.

$$\begin{aligned} Y_{\mathrm{RaL}} = & -59.44 + 10.35 \times X_1 + 0.05 \times X_2 + 5.83 \times X_3 + 262.35 \times X_4 \\ & - 0.55 \times X_1^2 - 1.25 \times X_3^2 - 7203.72 \times X_4^2 + 0.08 \times X_1 X_3 \\ & - 28.54 \times X_1 X_4 + 0.20 \times X_2 X_4 + 29.94 \times X_3 X_4 \end{aligned} \tag{3}$$

$$\begin{aligned} Y_{\mathrm{RaT}} = & -24.08 + 6.79 \times X_1 + 0.01 \times X_2 + 4.13 \times X_3 \\ & - 47.01 \times X_4 - 0.36 \times X_1^2 - 0.71 \times X_3^2 - 3416.52 \times X_4^2 \\ & - 0.23 \times X_1 X_3 + 5.96 \times X_1 X_4 + 0.10 \times X_2 X_4 + 34.31 \times X_3 X_4 \end{aligned} \tag{4}$$

$$\begin{aligned} Y_{\mathrm{RzL}} = & -313.5 + 50.4 \times X_1 + 0.3 \times X_2 + 34.4 \times X_3 \\ & + 1604.7 \times X_4 - 2.3 \times X_1^2 - 6.1 \times X_3^2 - 38642.1 \times X_4^2 \\ & - 0.1 \times X_1 X_3 - 143.0 \times X_1 X_4 + 1.2 \times X_2 X_4 + 28.1 \times X_3 X_4 \end{aligned} \tag{5}$$

Table 4 Experimental results of a total 31 experiments

Expt. No.	Responses				
	Surface roughness (lateral), Ra (μm)	Surface roughness (transverse), Ra (μm)	Surface roughness (lateral), Rz (μm)	Surface roughness (transverse), Rz (μm)	Contact angle, θ (degree)
1	11.75	6.91	61.06	37.49	52.60
2	5.02	4.99	29.86	25.60	115.10
3	6.98	7.11	42.46	35.99	76.55
4	8.68	6.32	47.05	33.03	25.00
5	11.50	8.25	59.66	41.66	102.00
6	3.68	3.62	21.54	20.11	15.10
7	13.66	9.91	72.54	48.15	67.30
8	7.32	4.56	40.50	23.55	30.30
9	12.70	7.73	65.42	38.95	53.30
10	4.91	4.55	31.62	23.80	132.45
11	7.53	5.22	40.15	25.63	82.40
12	6.07	4.86	36.60	29.20	38.90
13	12.06	7.35	72.18	37.43	26.70
14	9.84	7.41	53.13	34.30	75.15
15	5.13	5.32	33.60	31.14	31.40
16	10.23	7.57	53.91	35.80	25.90
17	11.10	7.62	55.45	39.12	71.55
18	10.25	8.62	60.59	40.54	51.25
19	3.57	3.58	24.16	18.48	95.95
20	6.25	5.32	40.50	27.22	73.20
21	9.73	7.18	52.22	39.17	117.85
22	10.64	9.53	57.04	45.85	48.65
23	11.93	8.18	68.73	42.35	55.10
24	3.82	3.95	24.27	20.94	80.50
25	13.86	9.65	74.94	46.47	22.10
26	12.88	7.07	72.90	39.37	26.60
27	14.64	9.62	75.54	48.81	31.10
28	6.97	7.08	38.36	35.41	82.70
29	5.70	5.82	32.43	28.82	91.90
30	7.50	4.70	42.53	25.50	32.20
31	10.25	7.17	53.76	34.08	21.30

$$\begin{aligned} Y_{\mathrm{RzT}} = & -135.2 + 32.5 \times X_1 + 0.1 \times X_2 + 20.6 \times X_3 \\ & + 166.8 \times X_4 - 1.7 \times X_1^2 - 2.5 \times X_3^2 - 22934.8 \times X_4^2 \\ & - 1.2 \times X_1 X_3 + 37.2 \times X_1 X_4 + 0.6 \times X_2 X_4 + 100.0 \times X_3 X_4 \end{aligned} \quad (6)$$

$$\begin{aligned} Y_\theta = {} & 103.38 + 37.30 \times X_1 - 0.20 \times X_2 - 106.27 \times X_3 \\ & + 1525.91 \times X_4 + 0.60 \times X_1^2 + 7.54 \times X_3^2 + 5793.90 \times X_4^2 \\ & - 0.04 \times X_1X_2 - 1.18 \times X_1X_3 - 376.04 \times X_1X_4 \\ & + 0.6 \times X_2X_3 + 0.65 \times X_2X_4 + 768.44 \times X_3X_4 \end{aligned} \quad (7)$$

Here, X_1, X_2, X_3, and X_4 are the actual values of laser beam average power, scanning speed, pulse frequency, and transverse feed, correspondingly. The analysis of variance (ANOVA) test for these four empirical models was performed and the calculated F-values are shown in Tables 5, 6, 7, 8 and 9 for surface roughness (lateral and transverse), Ra and Rz as well as contact angle (θ). The typical F-value of lack-of-fit is 4.06 for confidence level of 95% as taken from F distribution table. On the other hand, the evaluated F-values for surface roughness (lateral), surface roughness (transverse), and contact angle are 1.43, 0.97, 1.51, 1.11, and 1.66, respectively, at 95% confidence level. These calculated F-values are obviously lower than the typical F-value. This entails that the RSM-based empirical models are satisfactory at 95% confidence level and valid in the ranges of process parameters. The p-values of lack-of-fit for these five response criteria are 0.344, 0.542, 0.317, 0.471, and 0.276, which indicate the models adequately fit. Based on the developed empirical models of responses, further a total of eight validation

Table 5 Results of analysis of variance (ANOVA) for surface roughness (lateral), Ra

Source	DF	Seq SS	Adj SS	Adj MS	F	P
Regression	14	277.304	277.304	19.8074	6.63	0.000
Linear	4	156.766	47.670	11.9175	3.99	0.020
Square	4	111.445	111.445	27.8613	9.33	0.000
Interaction	6	9.093	9.093	1.5154	0.51	0.794
Residual error	16	47.800	47.800	2.9875		
Lack-of-fit	10	33.651	33.651	3.3651	1.43	0.344
Pure error	6	14.149	14.149	2.3581		
Total	30	325.104				

Table 6 Results of analysis of variance (ANOVA) for surface roughness (transverse), Ra

Source	DF	Seq SS	Adj SS	Adj MS	F	P
Regression	14	84.828	84.8277	6.0591	5.80	0.001
Linear	4	47.363	20.9190	5.2298	5.01	0.008
Square	4	31.280	31.2797	7.8199	7.49	0.001
Interaction	6	6.185	6.1852	1.0309	0.99	0.466
Residual error	16	16.714	16.7143	1.0446		
Lack-of-fit	10	10.321	10.3207	1.0321	0.97	0.542
Pure error	6	3.394	6.3935	1.0656		
Total	30	101.542				

Table 7 Results of analysis of variance (ANOVA) for surface roughness (lateral), Rz

Source	DF	Seq SS	Adj SS	Adj MS	*F*	*P*
Regression	14	6796.22	6796.22	485.44	6.42	0.000
Linear	4	3953.21	1207.27	301.82	3.99	0.020
Square	4	2555.70	2555.70	638.93	8.45	0.001
Interaction	6	287.31	287.31	47.88	0.63	0.702
Residual error	16	1209.48	1209.48	75.59		
Lack-of-fit	10	865.79	865.79	86.58	1.51	0.317
Pure error	6	343.69	343.69	57.28		
Total	30	8005.70				

Table 8 Results of analysis of variance (ANOVA) for surface roughness (transverse), Rz

Source	DF	Seq SS	Adj SS	Adj MS	*F*	*P*
Regression	14	1858.63	1858.63	132.759	7.01	0.000
Linear	4	1095.62	457.70	114.424	6.04	0.004
Square	4	644.14	644.14	161.036	8.50	0.001
Interaction	6	118.87	118.87	19.812	1.05	0.433
Residual error	16	302.97	302.97	18.936		
Lack-of-fit	10	196.43	196.43	19.643	1.11	0.471
Pure error	6	106.54	106.54	17.756		
Total	30	2161.60				

Table 9 Results of analysis of variance (ANOVA) for contact angle, θ

Source	DF	Seq SS	Adj SS	Adj MS	*F*	*P*
Regression	14	25543.9	25543.9	1824.56	4.78	0.002
Linear	4	17659.4	3886.7	971.69	2.55	0.080
Square	4	2283.4	2283.4	570.86	1.50	0.250
Interaction	6	5601.0	5601.0	933.50	2.45	0.072
Residual error	16	6106.2	6106.2	381.63		
Lack-of-fit	10	4485.1	4485.1	448.51	1.66	0.276
Pure error	6	1621.1	1621.1	270.18		
Total	30	31650.0				

experiments are carried out within the range of the process parameters considered in the present experimental work.

In Table 10, the process parametric settings considered for verification experiments are enlisted along with experimental result of responses. The comparative results between the experimental results and the RSM predicted results are shown in Table 11. The prediction errors have been calculated according to the following equation:

Table 10 Results of responses of verification experiments

Expt. No.	Process parameters				Responses obtained from experiments				
	Average power (W)	Pulse frequency (Hz)	Scanning speed (mm/s)	Transverse feed (mm)	Surface roughness (μm)				Contact angle (θ)
					Ra (L)	Ra (T)	Rz (L)	Rz (T)	
1	7	800	2	0.02	6.12	7.25	38.26	21.28	109.12
2	5.5	900	4	0.04	5.23	6.86	42.15	38.52	76.29
3	8.5	1100	2.5	0.01	5.75	9.56	53.46	42.15	54.28
4	5	1300	3.5	0.05	9.86	8.62	68.54	25.14	113.81
5	8	1200	2.5	0.02	4.62	7.91	72.13	37.29	80.18
6	9	950	3	0.03	8.25	5.26	35.16	37.21	95.25
7	6	700	4	0.01	8.46	4.85	47.91	47.29	76.15
8	8	1050	4.5	0.02	5.92	6.34	52.38	36.21	82.65

$$\text{Prediction error } (\%) = \frac{\text{Experimental results} - \text{Predicted results}}{\text{Experimental results}} \times 100\% \quad (8)$$

As shown in the Table 11, the predicted average percentage errors of surface roughness (lateral), surface roughness (transverse), and contact angle are 3.34, 3.19, 3.08, 3.10, and 3.19%, respectively. The calculated overall percentage of prediction error considering the aforesaid responses is 3.18%. As the prediction errors are below 5%, the result can be considered within acceptable range. In addition to this, the predicted values of responses are closed to experimental results, which ensure that RSM models developed can predict response results moderately acceptable.

4.2 Influence of Process Parameters on Surface Criteria

The various response surfaces have been plotted between one process criteria and two process parameters at a time. The parametric analyses of surface roughness (Ra and Rz) and contact angle with respect to process variables such as pulse frequency, average power, scanning speed, and transverse feed have been discussed hereunder.

4.2.1 Parametric Effects on Surface Roughness (Ra)

The influence of surface roughness (Ra and Rz) in lateral and transverse directions has been analyzed with the aid of various response surface plots. In Fig. 9, the combined effect laser beam average power and pulse frequency on surface roughness (Ra) in lateral direction is depicted when laser beam scanning speed and transverse feed are kept as constant at 3 mm/s and 0.03 mm, respectively. The surface plot reveals that an increment in laser beam average power, the surface roughness (lateral) values are increasing at all pulse frequency settings. This is due

Table 11 Results of verification experiments between the experiments and RSM prediction

Expt. No.	Experimental results					RSM predicted results					Prediction error (%)				
	Ra (L)	Ra (T)	Rz (L)	Rz (T)	(θ)	Ra (L)	Ra (T)	Rz (L)	Rz (T)	(θ)	Ra (L)	Ra (T)	Rz (L)	Rz (T)	(θ)
	(in μm)				(in degree)	(in μm)				(in degree)					
1	6.12	7.25	38.26	21.28	109.12	5.88	7.03	37.05	20.77	106.51	3.87	2.93	3.16	2.35	2.39
2	5.23	6.86	42.15	38.52	76.29	5.09	6.63	40.63	36.97	73.741	2.65	3.25	3.59	4.01	3.34
3	5.75	9.56	53.46	42.15	54.28	5.56	9.21	52.13	40.50	52.564	3.14	3.62	2.48	3.91	3.16
4	9.86	8.62	68.54	25.14	113.81	9.53	8.39	66.16	24.45	110.88	3.26	2.65	3.47	2.73	2.57
5	4.62	7.91	72.13	37.29	80.18	4.46	7.63	70.09	36.33	77.381	3.29	3.45	2.82	2.56	3.49
6	8.25	5.26	35.16	37.21	95.25	7.94	5.11	34.04	35.91	90.716	3.69	2.69	3.16	3.47	4.76
7	8.46	4.85	47.91	47.29	76.15	8.19	4.65	46.54	46.28	73.728	3.15	4.01	2.84	2.13	3.18
8	5.92	6.34	52.38	36.21	82.65	5.70	6.15	50.72	34.87	80.426	3.69	2.96	3.16	3.69	2.69
Average prediction error											3.34	3.19	3.08	3.10	3.19
General prediction error											3.18				

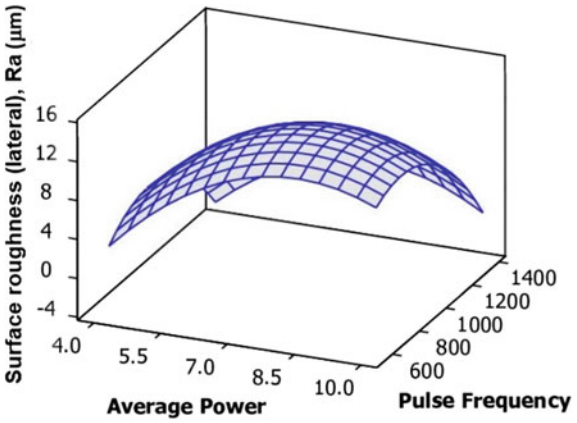

Fig. 9 3D surface plots of surface roughness (lateral), Ra against of average power and pulse frequency

to the fact that with increase of laser beam average power, the peak power of the beam is also increasing according to following equation (Kibria et al. 2012; Thawari et al. 2005):

$$\text{Peak power } (P_p) = \frac{\text{Average power } (P_A)}{\text{Pulse frequency } (F_p) \times \text{Pulse duration } (\mu)} \tag{9}$$

Thus, the material from the laser irradiated zone gets adequate energy to melt and evaporate instantly and as a result, the machined surface has a lot of irregularities. According to Eq. (1), the increase of pulse frequency for any change in laser beam scanning speed results in increase of lateral overlap percentage. Thus, the altitude of the micro-peaks on the generated surface is less, which further decreases the surface roughness (lateral) value. It is also seen from this figure that increment in pulse frequency first leads to increasing of the surface roughness (lateral) values and later reversed back. It is because, when pulse frequency is increasing, the laser beam interaction time with material surface is also increasing subsequently and thus, the crater size is also increasing. Consequently, the roughness values are increasing.

Figure 10 illustrates the influence of laser scanning speed and transverse feed on surface roughness (lateral) values when other process variables remained constant as beam average power at 7 W and laser pulse frequency at 1000 Hz. It is observed from the figure that with increase of laser beam scanning speed, initially roughness values have a tendency to increase and then follows a gradual fall. With increasing values of scanning speed, as the spot overlap values decreases, therefore, the roughness is increasing. At high scanning speed values, the laser beam and material interaction time decreases. As a result of this, slight quantity of work material is removed by laser beam irradiation and the surface has less irregularities. The same plot also depicts that with the increase of transverse feed, the values of surface roughness (lateral) are also increasing. This phenomenon is observed by the increase of transverse feed, where the values of transverse overlap between two

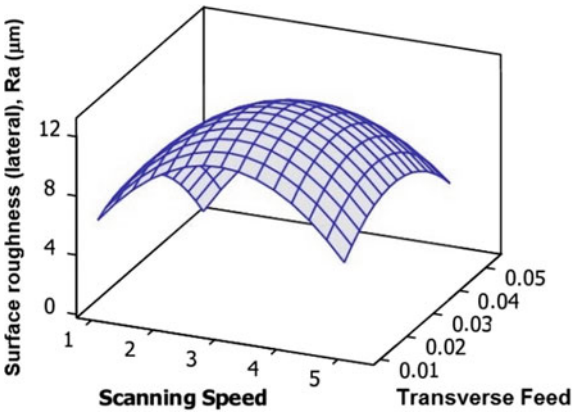

Fig. 10 3D surface plots of surface roughness (lateral), Ra against of scanning speed and transverse feed

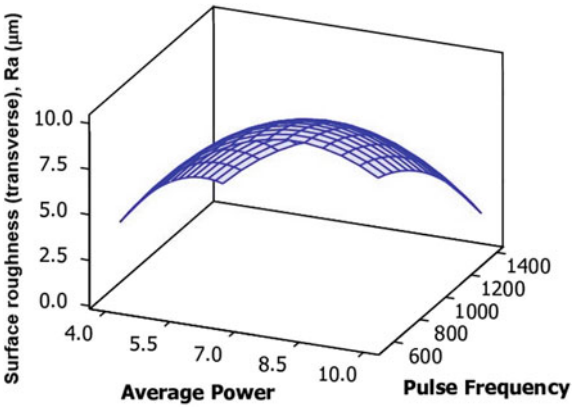

Fig. 11 3D surface plots of surface roughness (transverse), Ra against of average power and pulse frequency

laser scanning track decrease. Therefore, the machined surface has a lot of irregularities which ultimately increases the roughness.

Figure 11 shows the influence of laser beam average power and pulse frequency on surface roughness (transverse), Ra when other process parameters, i.e., scanning speed and transverse feed were kept constant at a value 3 mm/s and 0.03 mm, correspondingly. The figure reveals that surface roughness (transverse) shows an increasing trend with the variation of laser average power. This is due to the fact that when the average power is increasing, the peak power is also increasing according to Eq. (9). Thus, the material from the laser irradiated zone finds suitable thermal energy for melting and evaporation instantly and as a result, the machined surface has a lot of irregularities. The same plot also indicates that the surface roughness (transverse) values reduced with the variation of pulse frequency. This trend can be understood by Eq. (9) that shows with increasing pulse frequency, the peak power decreases, so the energy associated with the laser beam at the laser irradiated zone also decreases and less amount of metal is melted and vaporized

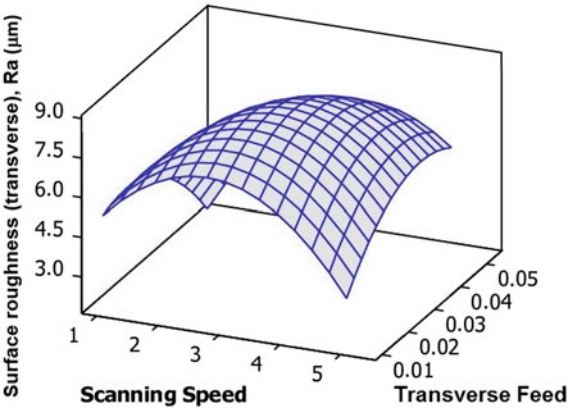

Fig. 12 3D surface plots of surface roughness (transverse), Ra against of scanning speed and transverse feed

from the zone. Therefore, irregularities with lower crater size are formed and the surface roughness value decreases.

Figure 12 shows the effects of surface roughness (transverse), Ra with the variation of scanning speed and transverse feed when the other two process parameters, i.e., laser beam average power and pulse frequency are kept constant at a value of 7 W and 1000 Hz. The figure depicts that surface roughness first gradually increases and then steep decreases with the increase of scanning speed parameter. This nature of the graph can be explained as when the scanning speed is increasing with constant average power and transverse feed, the overlap distance between the two consecutive lasers scanning track decreases. Therefore, the surface roughness also decreases. The same graph also depicts that the surface roughness (transverse) increases with the increasing of transverse feed. It is because according to Eq. (2), with increase of transverse feed, the values of transverse overlap between two laser scanning track decrease and thus, the machined surface has a lot of irregularities which ultimately increases the roughness.

4.2.2 Parametric Effects on Surface Roughness (Rz)

Figure 13 depicts the variation of surface roughness (lateral), Rz with laser average power and pulse frequency keeping other two process variables, i.e., scanning speed and transverse feed constant at a value of 3 mm/s and 0.03 mm, respectively. The graph indicates that the surface roughness values increase with laser beam average power. It is because of the increasing of peak power with the increase of laser beam average power according to Eq. (9). An increase value of peak power generates more energy in the laser zone and as a result of this, subsequent melting and vaporization takes place. Therefore, deeper layer of material is removed. This causes an increment in surface roughness. The same figure also depicts that the surface roughness (lateral) has a decreasing nature with the increment in pulse

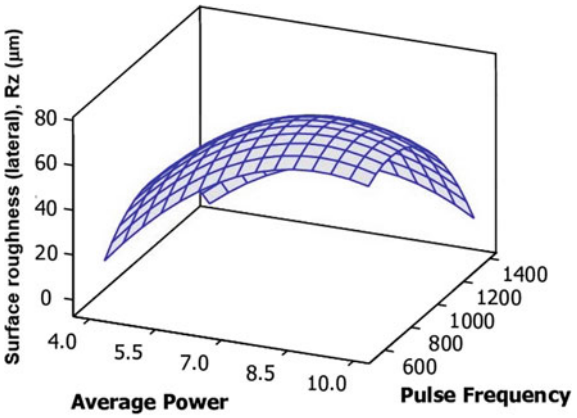

Fig. 13 3D surface plots of surface roughness (lateral), Rz against of average power and pulse frequency

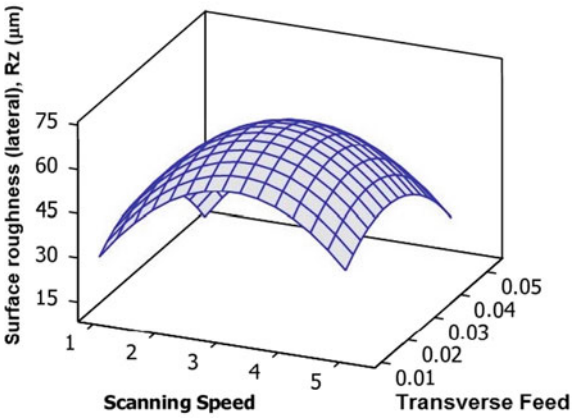

Fig. 14 3D surface plots of surface roughness (lateral), Rz against of scanning speed and transverse feed

frequency. Increased pulse frequency causes a decreasing peak power that further causes decrement in surface roughness.

Figure 14 shows the variation of surface roughness (lateral), Rz with scanning speed and transverse feed keeping the other two process parameters, i.e., laser average power and pulse frequency constant at 7 W and 1000 Hz, respectively. The figure shows a gradually increasing then followed by decreasing nature of the surface roughness curve with scanning speed. This is because, at lower value of scanning speed, the generated textured surface shows a decrease in overlap between the two spots and increased surface roughness. But, at high value of scanning speed, the duration of contact between laser beam and the material decreases significantly and it does not get enough time to melt and vaporize the material and as a result, the values of surface roughness decrease. The figure also shows that the surface roughness increases with increasing transverse feed. It is because with the increase of transverse feed, the values of transverse overlap between two laser

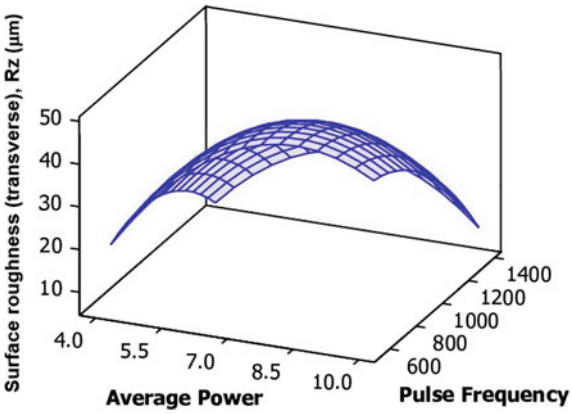

Fig. 15 3D surface plots of surface roughness (transverse), Rz against of average power and pulse frequency

scanning track decrease and thus, the machined surface has a lot of irregularities which ultimately increases the roughness.

Figure 15 illustrates the variation of surface roughness (transverse), Rz with beam average power and pulse frequency. The other two process parameters, i.e., scanning speed and transverse feed, are at constant at a value of 3 mm/s and 0.03 mm, respectively. The figure depicts that the surface roughness is increasing with beam average power. This is because the increased laser beam average power causes an increment in peak power and that generates more energy for melting and vaporization the work material. This causes the increasing of surface roughness. The same figure also shows that the surface roughness is decreasing when the pulse frequency goes on increasing as the peak power decreases with the increase in pulse frequency.

The variation of transverse surface roughness (Rz) with scanning speed and transverse feed is shown in Fig. 16, while laser beam average power and pulse frequency were kept constant at 7 W and 1000 Hz, correspondingly. The figure

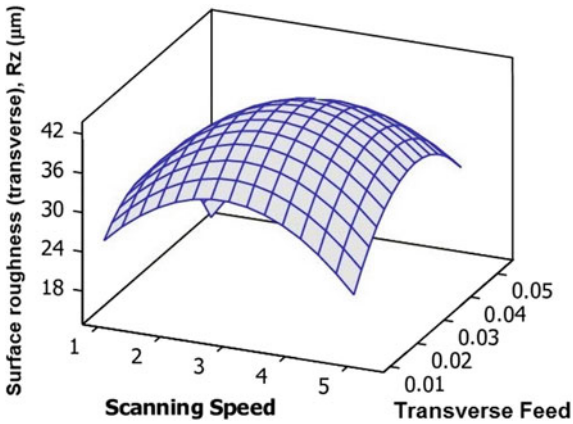

Fig. 16 3D surface plots of surface roughness (transverse), Rz against of scanning speed and transverse feed

shows a gradually increasing then decreasing nature of the surface roughness curve with scanning speed. This is because, at lower value of laser scanning speed, the generated textured surface shows decrease in overlap between the two spots and therefore, the surface roughness increases. But, at higher value of scanning speed, the interaction time between the laser beam and the work material decreases significantly without having enough time to melt and vaporize the material. As a result of this, the surface roughness decreases. The very same figure also shows that the surface roughness increases with increasing transverse feed. It is because with increase of transverse feed, the values of transverse overlap between two laser scanning track decrease and thus, the machined surface has lot of irregularities which ultimately increases the roughness.

4.2.3 Parametric Effects on Contact Angle (θ)

Figure 17 illustrates the variation of contact angle (θ) with beam average power and pulse frequency keeping other two process parameters, i.e., scanning speed and transverse feed, constant at 3 mm/s and 0.03 mm correspondingly. It is obvious from the surface plot that with increment of average power of laser, it has small effect on contact angle when pulse frequency value is less. However, at high value of pulse frequency settings, the contact angle sharply decreases. Consequently, the wettability between water drop and machined surface increases. It is also observed that at less value of laser beam average power, with increase of pulse frequency, contact angle increases sharply and consequently the wettability of the surface with water drop decreases.

Figure 18 illustrates the variation of contact angle (θ) with pulse frequency and scanning speed when laser beam average power and transverse feed remained constant at 1000 Hz and 0.03 mm correspondingly. The surface plot reveals that with the combination of low scanning speed and high values of pulse frequency, the changes in contact angle are minimal. On the contrary, at high scanning speed with

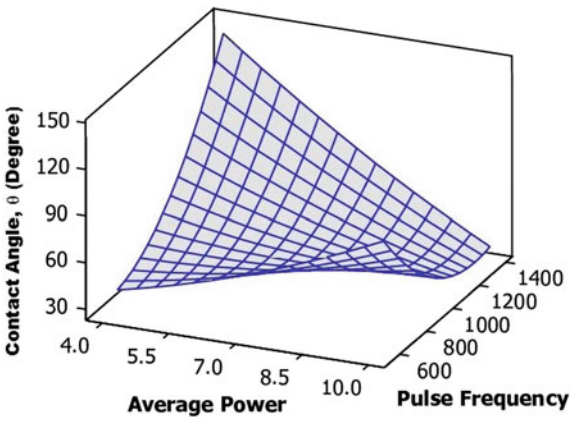

Fig. 17 3D surface plots of contact angle against of average power and pulse frequency

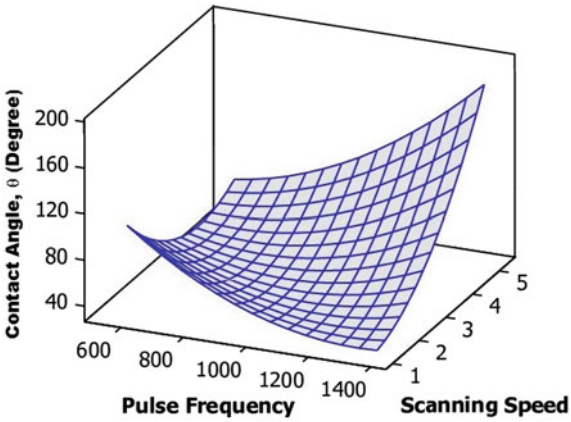

Fig. 18 3D surface plots of contact angle against of pulse frequency and scanning speed

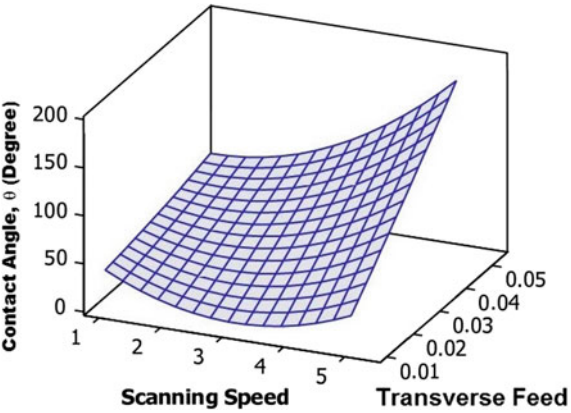

Fig. 19 3D surface plots of contact angle against of scanning speed and transverse feed

increasing pulse frequency contact angle increases and the wettability decreases. Simultaneously, at low pulse frequency, increasing of scanning speed has a very small effect on contact angle, but at high pulse frequency, increment in scanning speed causes the contact angle to increase sharply. From the plot, it is optimized that the contact angle has minimum value at higher value of pulse frequency and lower value of scanning speed. On the other hand, the contact angle has a maximum value at higher value of pulse frequency as well as scanning speed.

Figure 19 shows the variation of contact angle (θ) with scanning speed and transverse feed while remaining other process parameters such as laser beam average power and pulse frequency constant at 7 W and 1000 Hz, correspondingly. The surface plot of the contact angle against these two parameters shows that with the increase of scanning speed, the contact angle increases sharply at all value of transverse feed. This makes the surface hydrophobic in nature. At the same time, with increase of transverse feed, the value of contact angle has an increasing nature at all values of scanning speed. Thus, wettability of the surface against water drop decreases.

5 Multi-objective Optimization and Validation Experiments

For obtaining minimum values of surface roughness (Ra and Rz) and contact angle (θ), it is very essential to consider optimization statistical tool to achieve multi-objective optimization parametric combination of considered process parameters. Figure 20 shows the result of the optimized combination of the process variables in order to achieve the optimized tribological characteristics. In the aforesaid figure, process parameters and their ranges are considered in columns, whereas the output responses are plotted in each row. Each cell in the figure also represents how the output response varies with one of the process parameters, while the other parameters are remained as constant. At an average power of 9.02 W, pulse frequency of 1340 Hz, laser beam scanning speed of 2.04 mm/s, and transverse feed of 0.0227 mm, the optimal settings of the process parameters are

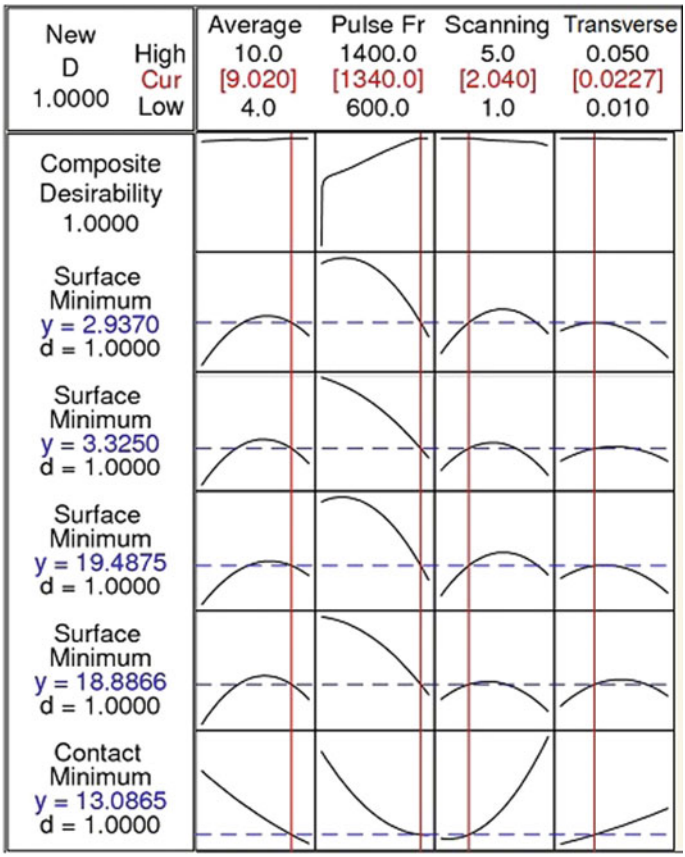

Fig. 20 Multi-objective optimization results of responses

achieved. The optimal surface roughness (lateral), Ra achieved was 2.93 μm, surface roughness (transverse), Ra 3.32 μm, surface roughness (lateral), Rz 19.48 μm, surface roughness (transverse), Rz 18.89 μm, contact angle (θ) 13.08°. With the composite desirability (D) value of 1, all the responses have been successfully optimized during multi-objective optimization.

Verification experiment of confirming the values of multi-objective optimization was conducted at the closer achievable parametric combination of multi-objective optimized setting. The RSM predicted and experimental results of responses with the percentage of prediction errors are shown in Table 12. It has been found that the optimum values of surface roughness (lateral and transverse) and contact angle (θ) were obtained as 3.01, 3.44 20.13, 19.45 μm, and 13.53° respectively. The calculated values of prediction errors were 2.71, 3.43, 3.18, 2.87, and 3.31% as obtained using Eq. (8). These values are within acceptable limit. Thus, the optimized parametric combination is valid within considered range of process parameters.

Table 12 Results of optimal parametric combinations and confirmation experiments

Optimization	Experimental parameters settings	Experimental results
Multi-objective optimization	Average power = 9.02 W Pulse frequency = 1340 Hz Scanning speed = 2.04 mm/s Transverse feed = 0.0227 mm	Surface roughness (lateral), Ra = 3.01 μm, Surface roughness (transverse), Ra = 3.44 μm Surface roughness (lateral), Rz = 20.13 μm Surface roughness (transverse), Rz = 19.45 μm Contact angle (θ) = 13.53° **RSM predicted results** Surface roughness (lateral), Ra = 2.93 μm, Surface roughness (transverse), Ra = 3.32 μm Surface roughness (lateral), Rz = 19.48 μm Surface roughness (transverse), Rz = 18.89 μm Contact angle (θ) = 13.08° **Percentage of error (%)** Surface roughness (lateral), Ra = 2.71 Surface roughness (transverse), Ra = 3.43 Surface roughness (lateral), Rz = 3.18 Surface roughness (transverse), Rz = 2.87 Contact angle (θ) = 3.31

6 Analysis of Optical Microscopic Images of Laser Textured Surfaces

Studies of optical microscopic images of textured surface machined at various parametric settings have been done in depth for investigating the influences of process parameters. Figure 21a–d show and compare the laser textured surfaces machined at parametric combinations of (a) and (b) 5.5 W/1200 Hz/2 mm/s/0.02 mm and 5.5 W/1200 Hz/4 mm/s/0.04 mm of average power, pulse frequency, scanning speed, and transverse feed. By closely observing these optical micrographs in Fig. 21a–d, it is seen that with the combination of higher value of laser scanning speed and transverse feed, the values of surface roughness (lateral and transverse) were increased from Ra = 3.68 μm and Ra = 3.62 μm to Ra = 4.91 μm and Ra = 4.55 μm. The corresponding values of surface roughness (lateral and transverse) were increased from Rz = 21.54 μm and Rz = 20.11 μm to Rz = 31.62 μm and Rz = 23.80 μm. The increase of surface roughness (both lateral and transverse) is due to decrease in lateral and transverse overlaps with laser beam scanning speed and transverse feed. Figure 22a–d shows and compare the laser

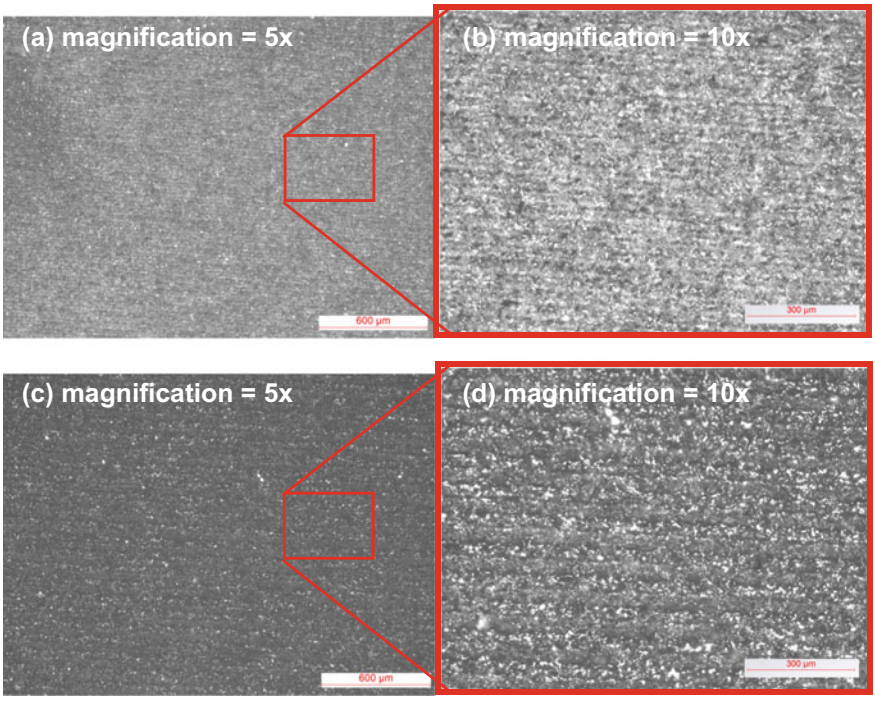

Fig. 21 Optical micrographs of laser textured surface machined at **a**, **b** 5.5 W/1200 Hz/2 mm/s/0.02 mm, **c**, **d** 5.5 W/1200 Hz/4 mm/s/0.04 mm of average power, pulse frequency, scanning speed and transverse feed

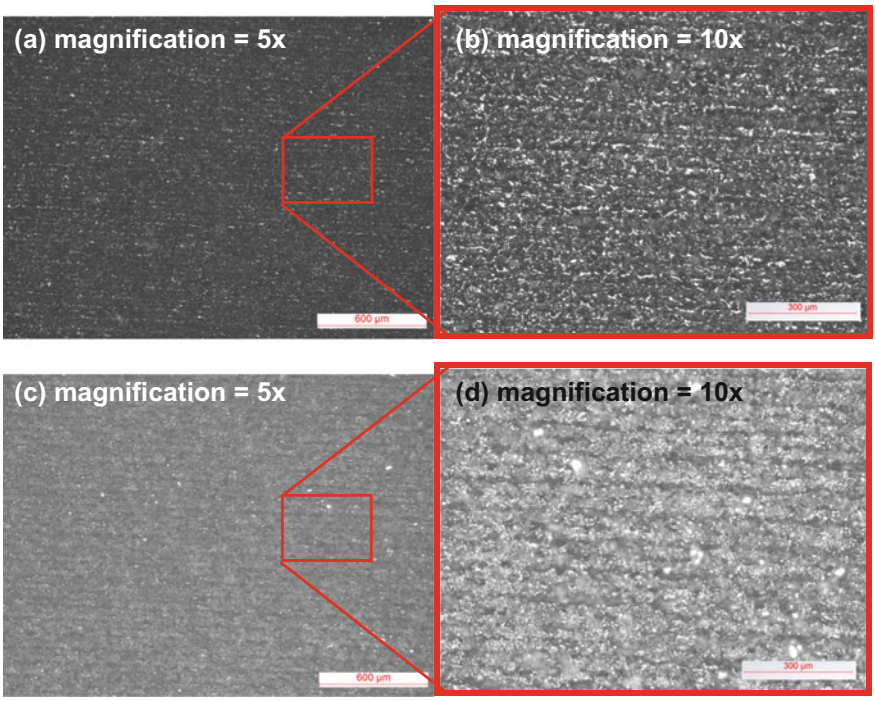

Fig. 22 Optical micrographs of laser textured surface machined at **a** and **b** 5.5 W/1200 Hz/2 mm/s/0.04 mm, **c**, **d** 8.5 W/800 Hz/2 mm/s/0.04 mm of average power, pulse frequency, scanning speed and transverse feed

textured surfaces machined at parametric combinations of (a) and (b) 5.5 W/1200 Hz/2 mm/s/0.04 mm and 8.5 W/800 Hz/2 mm/s/0.04 mm of average power, pulse frequency, scanning speed, and transverse feed. By closely observing these optical micrographs, it is seen that with the increase of laser beam average power and decrease of pulse frequency, the values of surface roughness (lateral and transverse) were decreased from Ra = 6.98 μm and Ra = 7.11 μm to Ra = 3.57 μm and Ra = 3.58 μm. The corresponding values of surface roughness (lateral and transverse) were decreased from Rz = 42.46 μm and Rz = 35.99 μm to Rz = 24.16 μm and Rz = 18.48 μm. The decrease of surface roughness (both in lateral and transverse) with an increase in average power and decrease in pulse frequency is due to increase in laser–material interaction time and eventually the formation of craters on the textured surfaces.

Figure 23 shows the photographic views of water droplets on laser textured surfaces machined at six different parametric combinations. These images have been taken utilizing the indigenously developed contact angle measuring arrangement as explained in Fig. 8. The figures also show the values of contact angle produced due to contact of solid titanium machined surface as well as due to surface tension for surrounding air. As the values of contact angle of water droplets shown

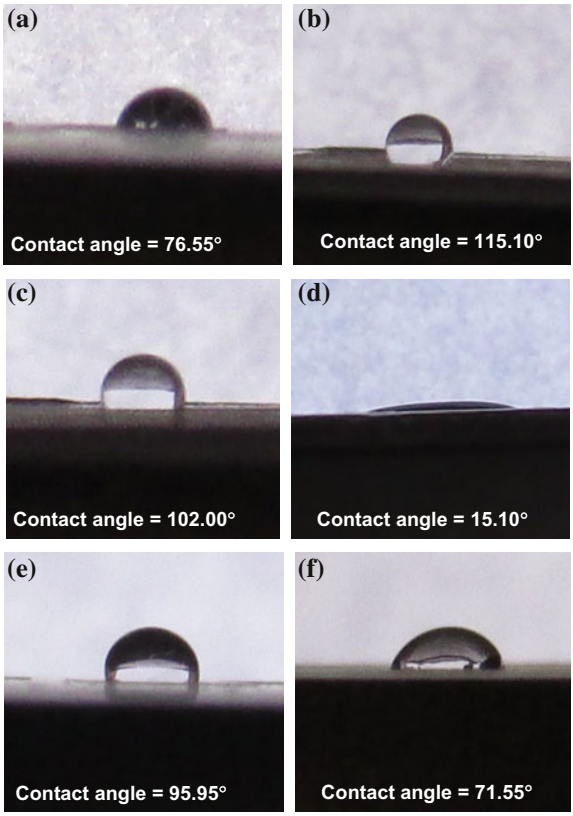

Fig. 23 Photographic views of water droplets on the laser textured surface machined at **a** 8.5 W/800 Hz/2 mm/s/0.04 mm, **b** 8.5 W/1200 Hz/4 mm/s/0.04 mm, **c** 8.5 W/800 Hz/4 mm/s/0.04 mm, **d** 5.5 W/1200 Hz/2 mm/s/0.02 mm, **e** 5.5 W/1200 Hz/2 mm/s/0.04 mm, and **f** 7 W/1000 Hz/3 mm/s/0.03 mm of average power, pulse frequency, scanning speed, and transverse feed

in Fig. 23b, c, e are 115.10°, 102.00°, and 95.95°, which are more than 90°, therefore, these machined surfaces can be termed as hydrophobic surface (wettability low). However, the machined surfaces shown in Fig. 23a, d, f create contact angles of water droplets as 76.55°, 15.10°, and 71.55°, which are less than 90°, therefore, these machined surfaces can be termed as hydrophilic surface (wettability high).

7 Conclusions

In the present chapter, the effect of various process parameters on laser surface texturing tribological characteristics of commercially pure titanium sheet (thickness of 1 mm) is investigated and analyzed subsequently. Further, development of empirical models was conducted to correlate the process parameters and various responses. Based on the experimental results obtained, the mathematical models of the responses have been developed. With analysis of variance (ANOVA) test, these

models were validated statistically at 95% confidence level. Analysis of various surface plots reveals that all the parameters, i.e., laser beam average power, pulse frequency, scanning speed, and transverse feed have significant influences to achieve quality surface and defined wettability. Scanning speed and pulse frequency are the most significant and contributing parameters for surface roughness (Ra and Rz) in lateral direction, whereas scanning speed and traverse feed are the most relevant and contributing parameters for surface roughness (Ra and Rz) in transverse direction. Multi-objective optimization parametric combination was also obtained for achieving least surface roughness (Ra and Rz) in lateral and transverse directions. Optimized response values are achieved such as surface roughness (lateral), Ra of 2.93 μm, surface roughness (transverse), Ra of 3.32 μm, surface roughness (lateral), Rz of 19.48 μm, surface roughness (transverse), Rz of 18.89 μm, and contact angle (θ) of 13.08° at the parametric setting of average power at 9 W, pulse frequency at 1400 Hz, laser beam scanning speed at 2 mm/s, and transverse feed at 0.02 mm. The results of verification experiments show that the prediction errors are within acceptable limits. The experimental results achieved in this research will be useful in developing new strategies and guidelines for research scientists and manufacturing engineers for more exploration in this area of surface texturing process using laser beam on titanium material. Furthermore, this research will provide great impetus for effective and successful utilization of pulsed Nd:YAG laser during the tribological surface generation of specific surface properties for successful applications in the micro-parts manufacturing.

References

Ali, M.Y., and W.N.P. Hung. 2017. Micromachining. In *Comprehensive materials finishing*, ed. S. Hashmi, vol. 1: *Finish machining and net-shape forming*, 322–343. Elsevier.

Chang, C.W., C.Y. Chen, T.L. Chang, C.J. Ting, C.P. Wang, and C.P. Chou. 2012. Sapphire surface patterning using femtosecond laser micromachining. *Applied Physics A* 109 (2): 441–448.

Chavoshi, S.Z., and X. Luo. 2015. Hybrid micro-machining processes: A review. *Precision Engineering* 41: 1–23.

Cunha, A., V. Oliveira, and R. Vilar. 2016. Ultrafast laser surface texturing of titanium alloys. In *Laser surface modification of biomaterials: Techniques and applications*, 301–322. Woodhead Publishing.

Dunn, A., K.L. Wlodarczyk, J.V. Carstensen, E.B. Hansen, J. Gabzdyl, P.M. Harrison, J.D. Shephard, and D.P. Hand. 2015. Laser surface texturing for high friction contacts. *Applied Surface Science Part B* 357: 2313–2319.

Gentili, E., L. Tabaglio, and F. Aggogeri. 2005. Review on micromachining techniques. In *AMST'05 advanced manufacturing systems and technology*, vol. 486, 387–396. Vienna: CISM International Centre for Mechanical Sciences, Springer.

Jackson, M.J., M.D. Whitfield, G.M. Robinson, R.G. Handy, J.S. Morrell, W. Ahmed, and H. Sein. 2015. Micromachining from a materials perspective. In *Machining with nanomaterials*, 77–127. Switzerland: Springer International Publishing.

Kibria, G., B. Doloi, and B. Bhattacharyya. 2012. Optimisation of Nd:YAG laser micro-turning process using response surface methodology. *International Journal of Precision Technology* 3 (1): 14–36.

Kibria, G., B. Doloi, and B. Bhattacharyya. 2015. Pulsed Nd:YAG laser micro-turning process of alumina ceramics. In *Lasers based manufacturing*, ed. Shrikrishna N. Joshi, and Uday Shanker Dixit, 343–380. India: Springer.

Kovalchenko, A., O. Ajayi, A. Erdemir, G. Fenske, and I. Etsion. 2004. The effect of laser texturing of steel surfaces and speed-load parameters on the transition of lubrication regime from boundary to hydrodynamic. *Tribology Transactions* 47 (2): 299–307.

Li, B.J., H. Li, L.J. Huang, N.F. Ren, and X. Kong. 2016. Femtosecond pulsed laser textured titanium surfaces with stable superhydrophilicity and superhydrophobicity. *Applied Surface Science* 389: 585–593.

Meijer, J. 2004. Laser beam machining (LBM), state of the art and new opportunities. *Journal of Materials Processing Technology* 149: 2–17.

Mishra, S., and V. Yadava. 2015. Laser beam micro machining (LBMM)—A review. *Optics and Lasers in Engineering* 73: 89–122.

Soveja, A., E. Cicala, D. Grevey, and J.M. Jouvard. 2008. Optimisation of TA6 V alloy surface laser texturing using an experimental design approach. *Optics and Lasers in Engineering* 46 (9): 671–678.

Thawari, G., J.K.S. Sundar, G. Sundararajan, and S.V. Joshi. 2005. Influences of process parameters during pulsed Nd:YAG laser cutting of nickelbase superalloys. *Journal of Materials Processing Technology* 170 (1–2): 229–239.

Toyserkani, E., and N. Rasti. 2014. Ultrashort pulsed laser surface texturing. In *Laser surface engineering*, ed. D. Waugh, and J. Lawrence, 441–453. Woodhead Publishing.

Tripathi, K., B. Joshi, G. Gyawali, A. Amanov, and S.W. Lee. 2015. A study on the effect of laser surface texturing on friction and wear behavior of graphite cast iron. *Journal of Tribology* 138 (1): 011601–011610.

Velasquez, T., P. Han, J. Cao, and K.F. Ehmann. 2013. Feasibility of laser surface texturing for friction reduction in surgical blades. In *Proceedings of the ASME 2013 international manufacturing science and engineering conference*, V001T01A009. Madison, Wisconsin, USA.

Vora, H.D., and N.B. Dahotre. 2015. Surface topography in three-dimensional laser machining of structural alumina. *Journal of Manufacturing Processes* 19: 49–58.

Wang, X., Y. Xing, and M. Giovannini. 2015. Effect of overlap and overscan number in laser surface texturing of medical needles. *Applied Physics A* 120 (1): 229–238.

Yang, C.J., X.S. Mei, Y.L. Tian, D.W. Zhang, Y. Li, and X.P. Liu. 2016. Modification of wettability property of titanium by laser texturing. *International Journal of Advanced Manufacturing Technology* 87 (5): 1663–1670.